Supplementary Materials for

Taxel-Addressable Matrix of Vertical-Nanowire Piezotronic Transistors for Active/Adaptive Tactile Imaging

Wenzhuo Wu, Xiaonan Wen, Zhong Lin Wang*

*To whom correspondence should be addressed. E-mail: zhong.wang@mse.gatech.edu

Published 25 April 2013 on *Science* Express
DOI: 10.1126/science.1234855

This PDF file includes:

MATERIALS AND METHODS:

Processing scheme for fabricating 3D vertical piezotronic transistors array

Substrate preparation

1. Clean the Polyethylene terephthalate (PET) substrate or silicon wafer (acetone, isopropyl alcohol (IPA), deionized (DI) water).
2. Deposit a thin layer of SiO_2 (30 nm) to the substrate via electron-beam evaporation.

Bottom electrode formation

3. Spin-coat negative-tone photoresist (Futurrex NR9-1500PY) onto the substrates and soft-bake at 150 ^{o}C for 60 s.
4. Expose the samples with 365 nm UV lithography using first layer pattern.
5. Post-bake the samples at 100 ^{o}C for 60 s.
6. Develop the exposed samples in aqueous base developer (Futurrex Resist Developer RD6).
7. Rinse and blow-dry the samples.
8. Deposit 150 nm ITO as the bottom electrodes through RF magnetron sputtering.
9. Immediately deposit 3 nm Cr onto the ITO electrodes through electron beam evaporation.
10. Lift-off ITO/Cr in acetone.

Bottom Schottky contact formation and active area defining

11. Clean the processed samples in step 10 (acetone, IPA, DI water).
12. Pattern photoresist using second layer mask (steps 3-7).

13. Deposit 20 nm Au through electron beam evaporation.

14. Deposit 100 nm ZnO through RF magnetron sputtering.

15. Lift-off Au/ZnO in acetone.

Synthesis of vertical ZnO NWs array

16. Clean the processed samples in step 15 (acetone, IPA, DI water).

17. Immerse the samples into the growth solution (25 mM $ZnCl_2$ and 25 mM Hexamethylenetetramine (HMTA, $(CH_2)_6N_4$)) at 85 ^oC for 6 hrs.

Encapsulation of vertical ZnO NWs array

18. Clean the processed samples in step 17 (acetone, IPA, DI water).

19. Spin-coat encapsulation polymer (Microchem SU 8 2025) onto the samples.

20. Expose the samples with 365 nm UV lithography.

21. Cure the samples at 150 ^oC for 1 hr.

Exposure of top surfaces of ZnO NWs

22. Clean the processed samples in step 21 (acetone, IPA, DI water).

23. Dry etch the SU 8 layer in a reactive ion etcher.

24. Oxygen plasma treatment (50W, 180 mTorr, 15 minutes)

Top Schottky contact formation

25. Clean the processed samples in step 23 (acetone, IPA, DI water).

26. Pattern photoresist using second layer mask (steps 3-7).

27. Deposit 80 nm Au through electron beam evaporation.

28. Lift-off Au in acetone.

Top electrode formation

29. Clean the processed samples in step 27 (acetone, IPA, DI water).

30. Pattern photoresist using third layer mask (steps 3-7).

31. Deposit 150 nm ITO through RF magnetron sputtering.

32. Lift-off ITO in acetone.

33. Conformal Parylene C coating (1 μm thickness)

Multichannel multiplexed measurement

The electrical characterization platform interfaced with the 3D VSGPT array through a customized 200-pin probe card (Accuprobe Inc.) installed on the probe station (Cascade Microtech) (fig. S15). All of the 8464 taxels were individually-addressable by iteratively switching two multiplexer matrixes (NI PXI-2530) and output current from each SGVPT taxel under bias was measured and averaged within a short duration window of 10 ms by a 6½-digit digital multimeter (NI PXI-4072). The synchronized operations among the PXI modules as well as the data acquisition were controlled by the customized LabVIEW (National Instruments) code. The electrical characterization platform was connected to a computer for data registration and post-processing of acquired image. The background noise for the measurement system is also characterized and found to be significantly smaller than the measured responses (fig. S16).

Programmed mechanical inputs

A computer-controlled motorized 3-axis stage integrating with a force gauge (Dillon GL025) was used to apply normal load with well-defined magnitude at programmed locations on the device (fig. S15). The positioning of the 3-axis stage can be precisely controlled by software. Two of these linear stages control the position of the applied pressure (x and y coordinates) while

the third linear stage (vertical one in fig. S15) controls the magnitude of the applied pressure by varying z coordinate. The force gauge was used to monitor the magnitude of the applied pressure.

SUPPLEMENTARY FIGURES:

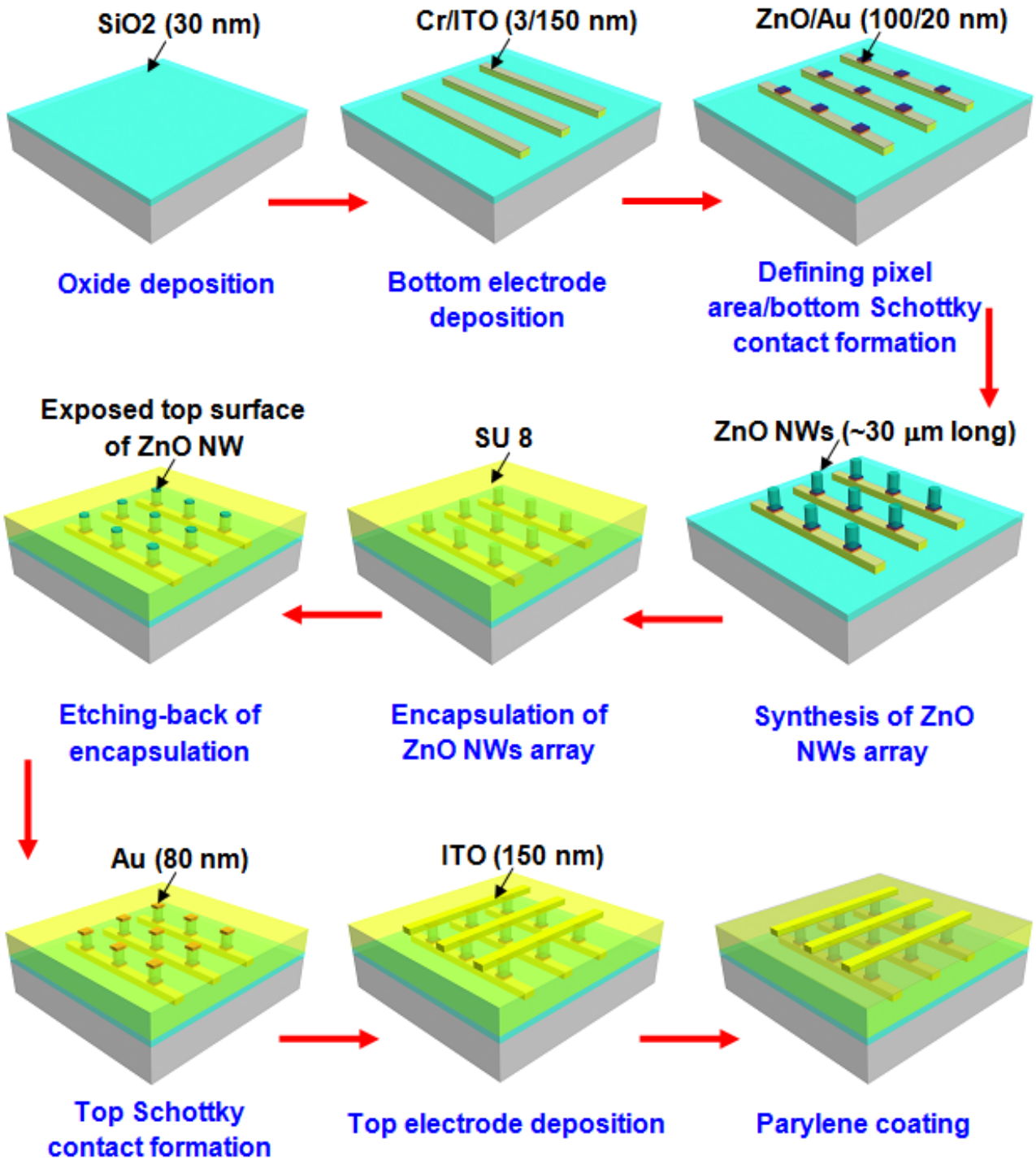

Figure S1: Schematic illustration of processing steps for fabricating 3D vertical piezotronic transistors array on a PET substrate.

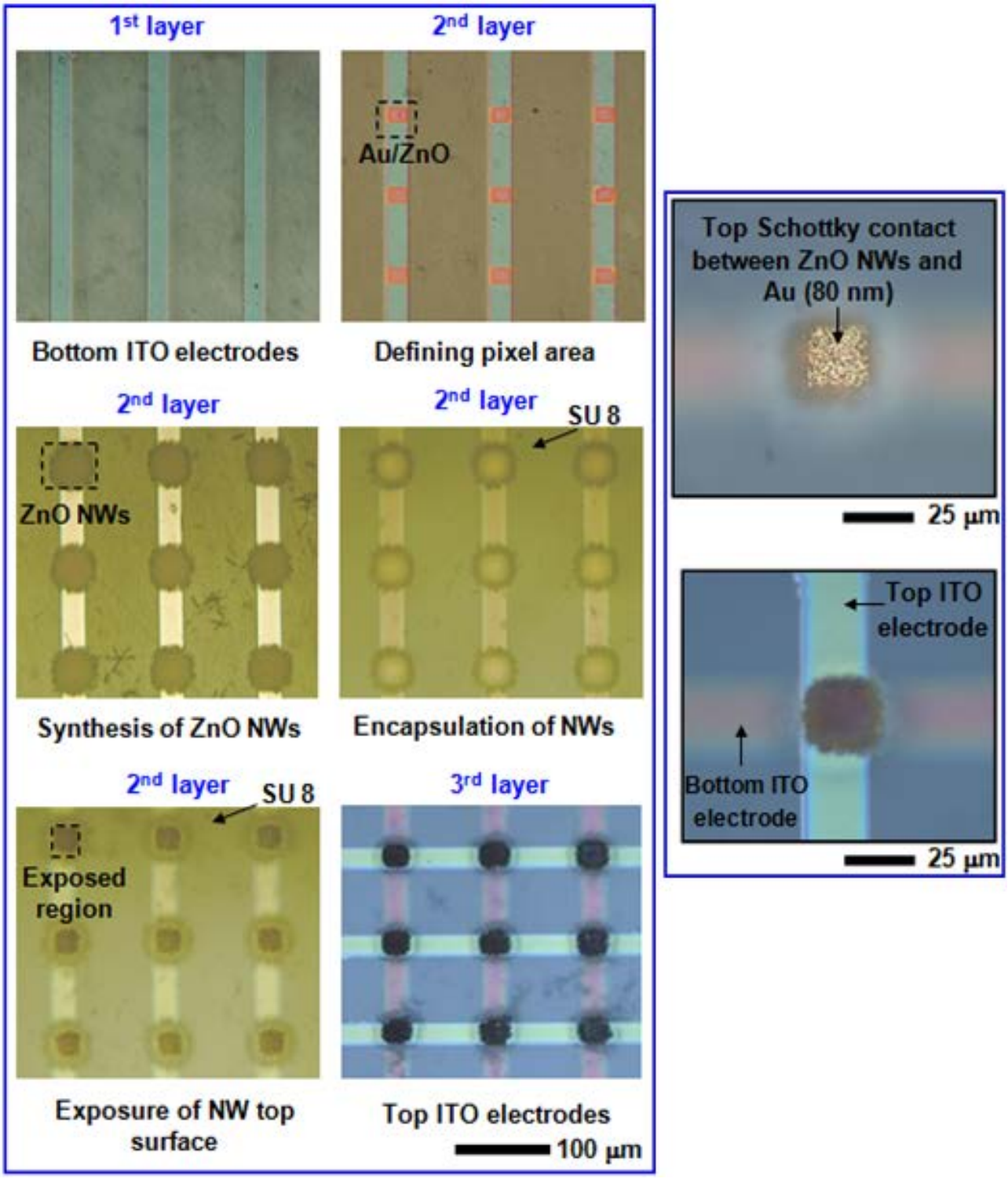

Figure S2: Left: Optical micrographs illustrating 3D vertical piezotronic transistors array on a PET substrate at each major step of fabrication process. **Right**: Magnified images of top Schottky contacts and single taxel after fabrication of 3rd layer electrode.

Materials characterization of the SGVPT array

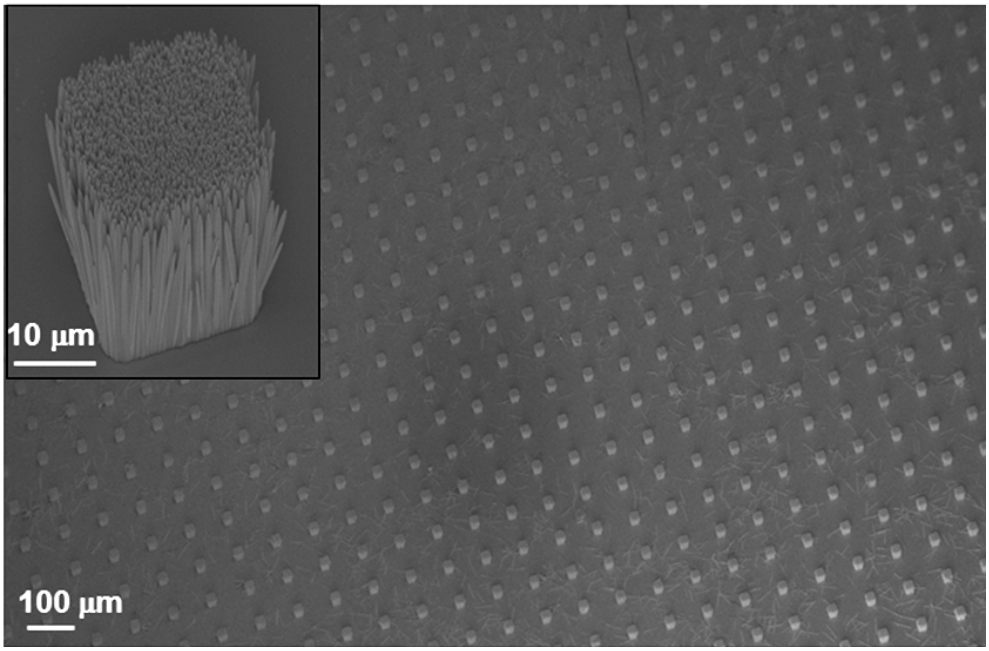

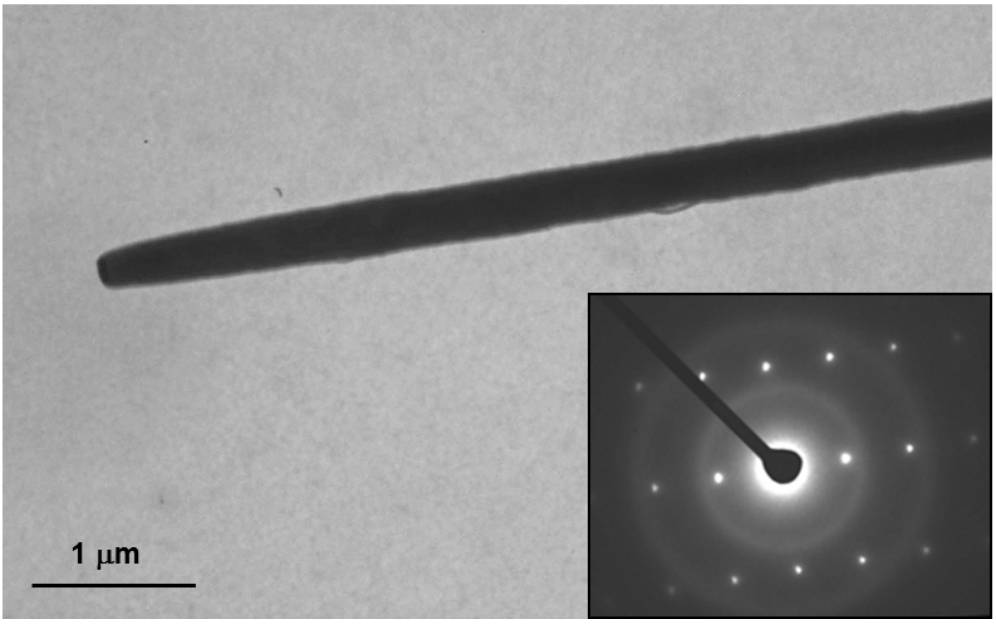

Figure S3: Top: 30^{o} tilted SEM image of 3D SGVPT array with top portions (~ 20 μm) of ZnO NWs (total length ~ 30 μm) exposed, showing the bunched growth of nanowires. **Bottom**: A TEM image and selective area electron diffraction (SAED) pattern from the nanowire, confirming its single-crystalline nature of the as-synthesized ZnO NWs from SGVPT array.

3D vertical piezotronic transistors array on flexible and transparent substrate

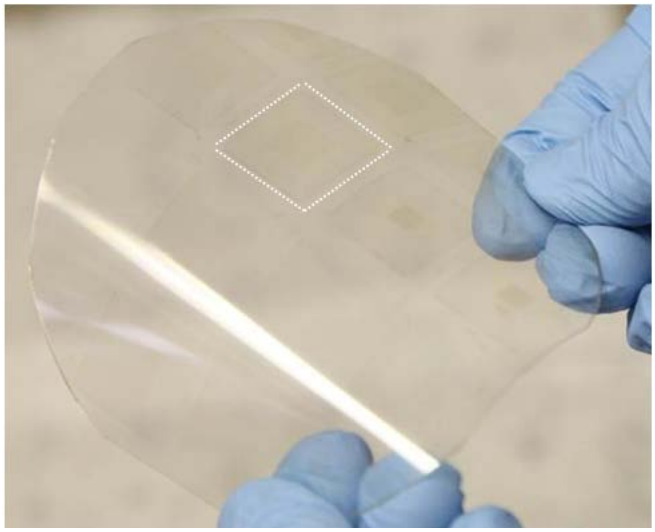

Figure S4: Image of 3D vertical piezotronic transistors arrays on a 4-inch PET substrate. Four configurations of array with different taxel densities and spacing are fabricated here using the processing steps described in Fig. S1. The region outlined by white dashed lines represents the device with taxel density of 92 x 92 in 1 cm^2.

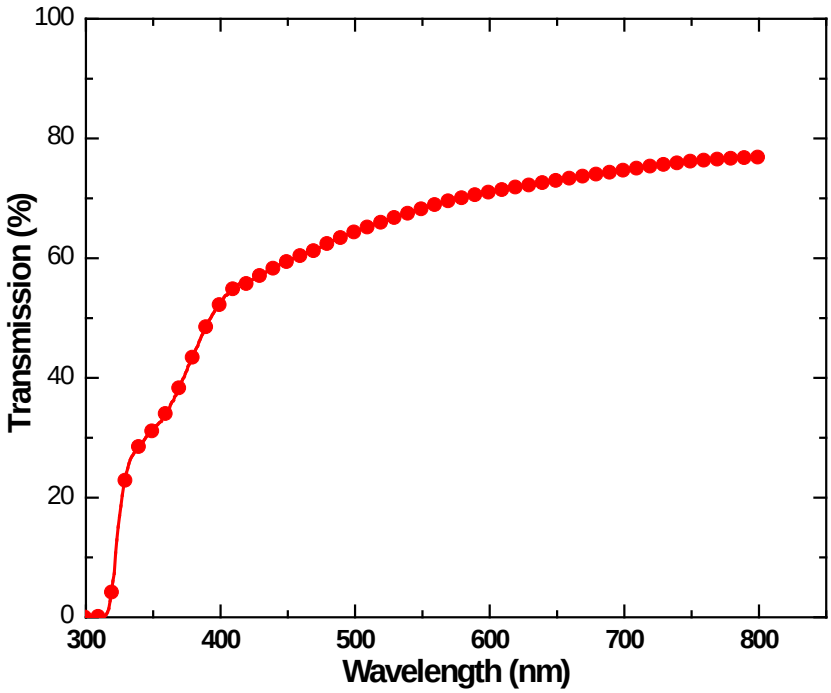

Figure S5: Measured normal incidence transmission (T) spectra of 3D vertical piezotronic transistors array (ITO/Cr/Au/ZnO NWs/Au/ITO: 150 nm/3 nm/20 nm/30 μm/80 nm/150 nm) on a PET substrate (~ 500 μm thick).

Piezotronic effect in SGVPT operation

When a ZnO NW device is under strain, there are two typical effects that may affect the carrier transport process. One is the piezoresistive effect because of the change in band gap, charge carrier density and possibly density of states in the conduction band of the semiconductor crystal under strain. This effect is a symmetric effect on the two end contacts and has no polarity, which will not produce the function of a transistor. Piezoresistance is a common feature of any semiconductors such as Si and GaAs and is not limited to the Wurtzite semiconductors. The other is the piezotronic effect because of the polarization of ions in a crystal that has non-central symmetry.

Piezotronic effect modulates characteristics of the two end contacts in an asymmetric or opposite manner, owing to the polarity of induced piezoelectric charges. The piezoelectric polarization charges are located at the ends of the NW (for c-axis grown ZnO), thus they directly affect the local contacts. In general, the negative piezoelectric polarization charges and hence the negative piezopotential induced at the semiconductor side near the interface of local contact formed between metal electrode and n-type semiconductor can repel the electrons away from the interface, resulting in further depleted interface and increased local barrier heights; while the positive piezoelectric polarization charges and hence the positive piezopotential created at the semiconductor side near the interface can attract the electrons towards the interface, resulting in less depleted interface and hence decreased local barrier heights. Piezopotential is therefore able to effectively modulate the local contact characteristics through an internal field, depending on doping type, carrier density and the crystallographic orientation of the piezoelectric semiconductor material as well as the polarity of the applied strain. Consequently, the transport of charge carriers across the metal-semiconductor contact can be effectively modulated by the piezoelectric polarization charges which can be controlled by varying the magnitude and polarity of externally applied strain. The modulation/gating of the charge transport across the interface by the strain-induced piezopotential is the core of piezotronics.

The data presented in Fig. S6 shows that piezotronic effect is the dominant mechanism in our SGVPT device.

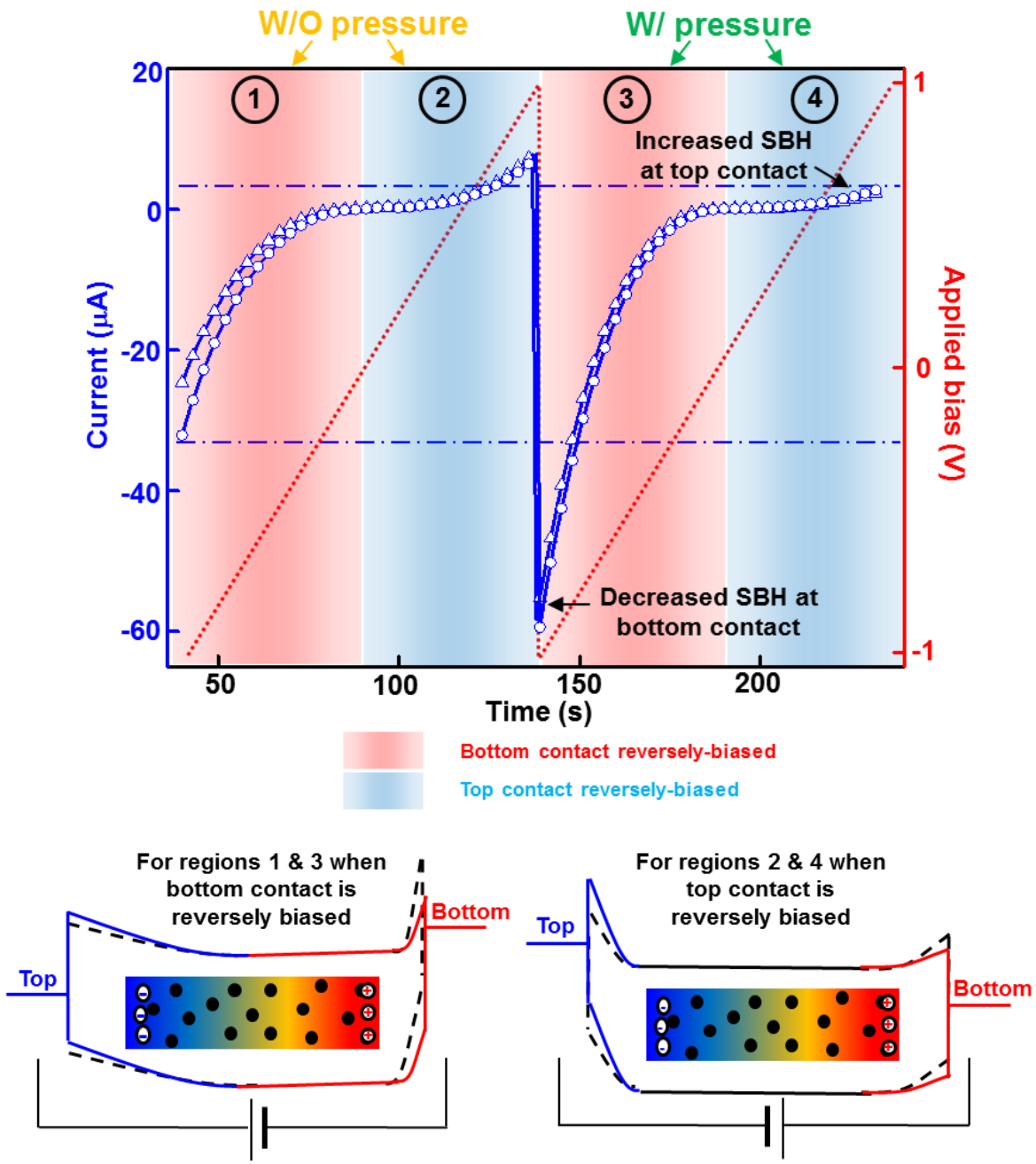

Figure S6: Experimental verification of piezotronic effect in operation of SGVPT devices. In the two-terminal SGVPT devices, the current flowing through the taxels is dedicated by the reversely-biased Schottky contact. Regions 1 and 3 (in red) correspond to the conditions when bottom Schottky contact is reversely biased, while regions 2 and 4 (in blue) correspond to the conditions when top Schottky contact is reversely biased. Sweeping I-V result (above) shows the asymmetric/opposite change

in magnitudes of current flowing through SGVPT taxels before and after strained (increased current when bottom contact is reversely-biased and decreased current when top contact is reversely-biased). This indicates that under the compressive strain, SBH at bottom Schottky contact is decreased (red solids lines in both band-diagrams shown above) and SBH at top Schottky contact is increased (blue solids lines in both band-diagrams shown above). This also matches the experimental facts that due to the polarity of induced strain (compressive) in SGVPT taxels by applied pressure and the crystallographic orientation of as-synthesized ZnO NWs, negative and positive piezoelectric polarization charges (symbols with “-” and “+” in the above band-diagrams) are induced at the top and bottom Schottky contacts respectively. The above observed sweep I-V result therefore confirms the piezotronic characteristics of the SGVPT taxel response. Responses from two taxels under pressure are plotted above (in open upper triangles and open circles). The same trend of current response has also been observed for other SGVPT taxels in the array. The color gradients in above band-diagrams indicate the distribution of piezopotential, with red representing positive piezopotential and blue representing negative piezopotential. Black-dashed lines in above band-diagrams represent the band profiles before external pressure is applied. Black-dots represent the charge carriers inside the NWs.

Response time of SGVPT taxel

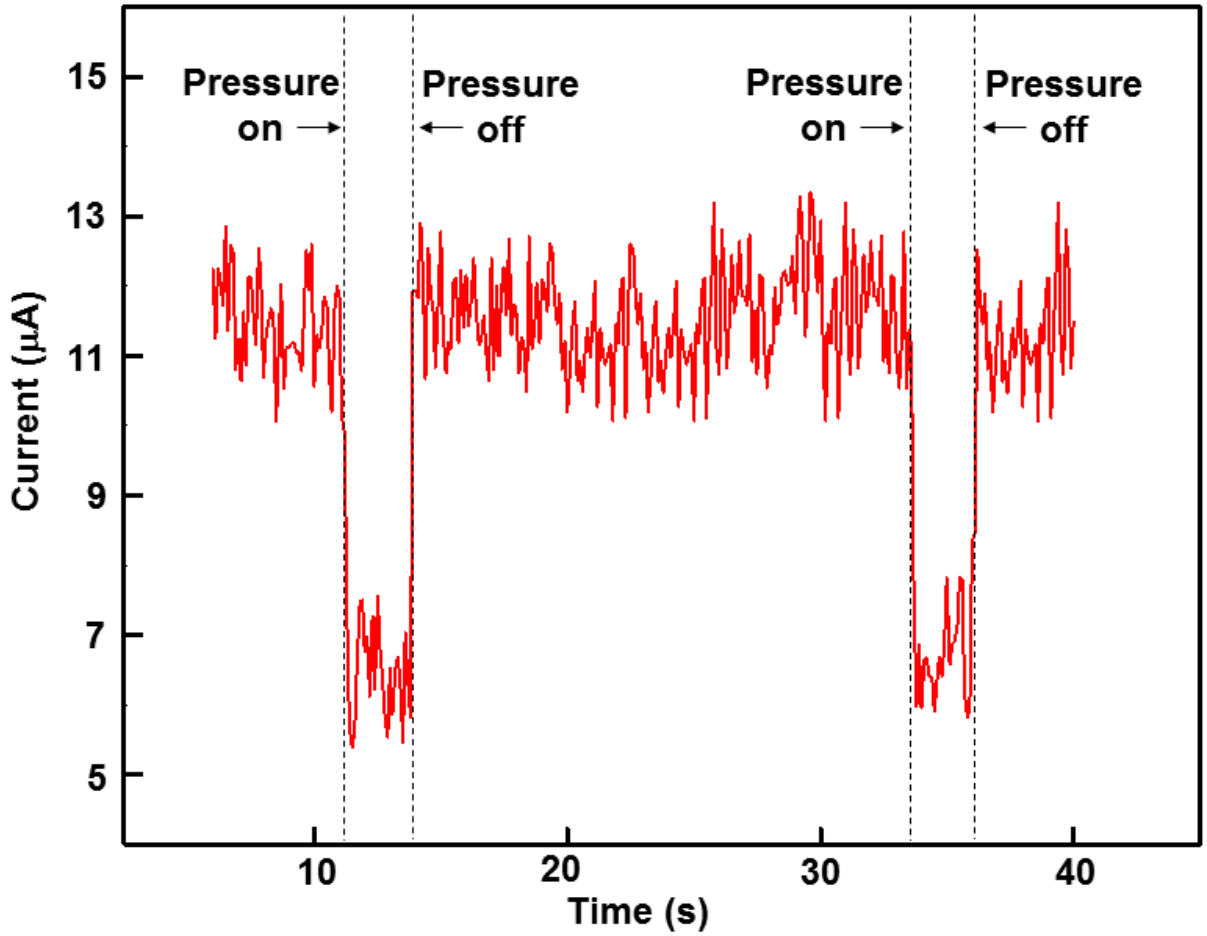

Figure S7: The measured response (rise) time for SGVPT taxel is around 0.15 s. The applied pressure is ~ 15 kPa.

Improvement of Schottky contact quality in SGVPT taxel by oxygen plasma treatment

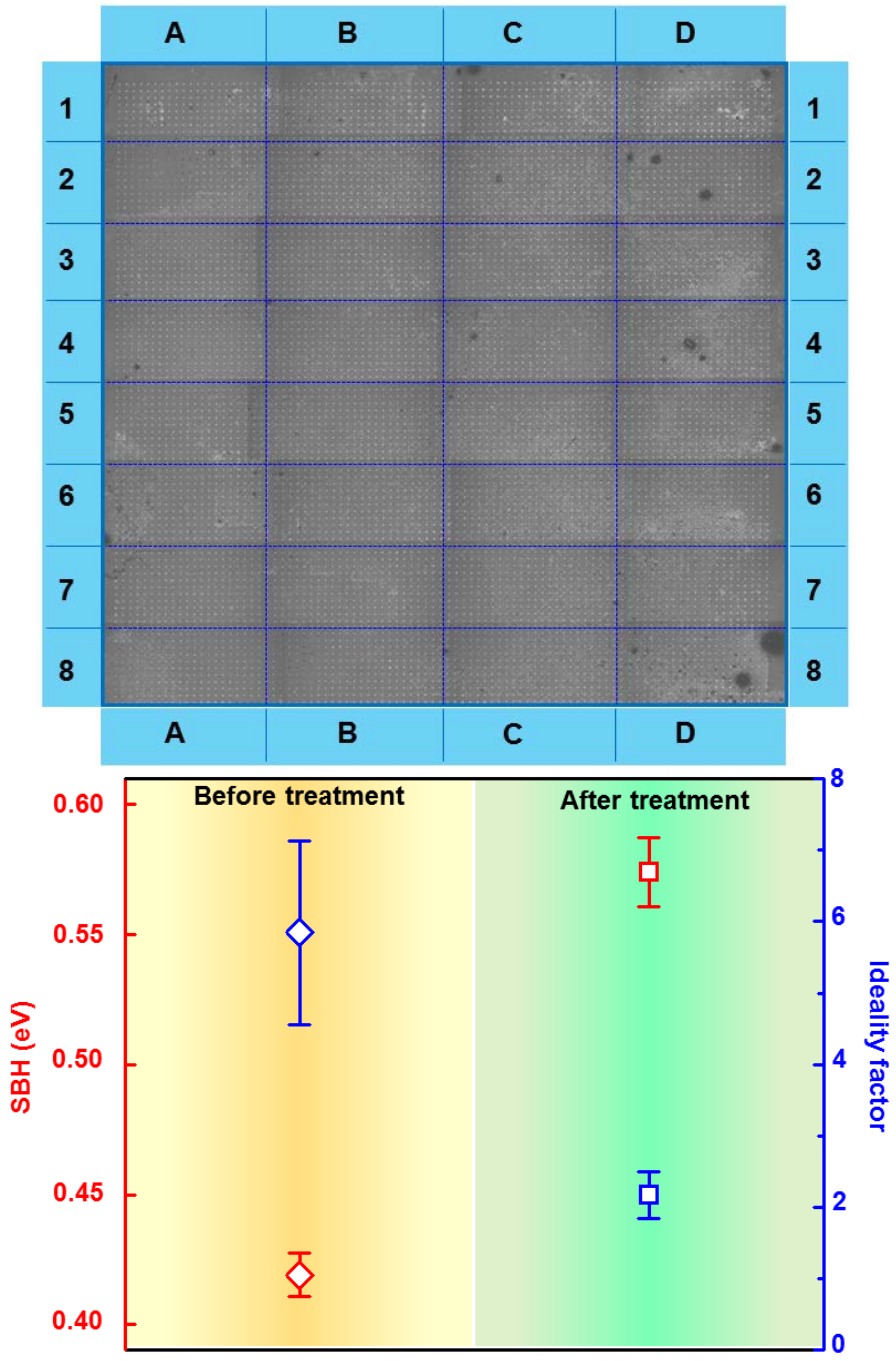

Figure S8: Top: Top view of the entire 92 x 92 SGVPT array, which has been divided into 32 regions. **Bottom**: Experimentally obtained Schottky barrier heights (SBHs) and ideality factors for 32 randomly selected taxels from the above 32 regions with (green region) and without (yellow region) oxygen plasma treatment, showing the significant improvement of Schottky contact quality in SGVPT taxels after the treatment.

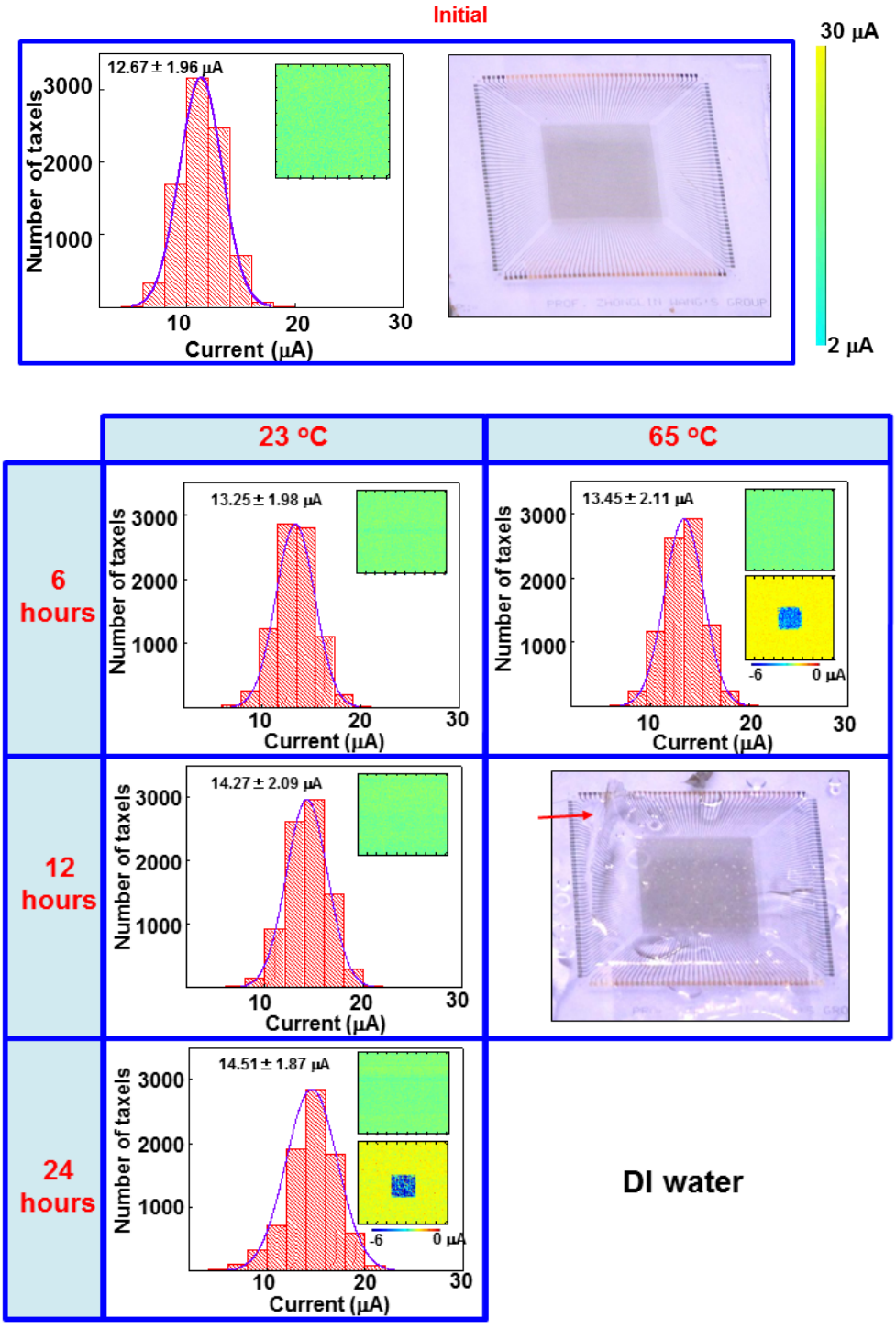

Figure S9: Aging effect of humidity on SGVPT array performance. The pressure applied for device after 24 hours immersion in 23 ^{o}C DI water and 6 hours in 65 ^{o}C DI water is ~ 15 kPa.

Humidity/environment test (continue)

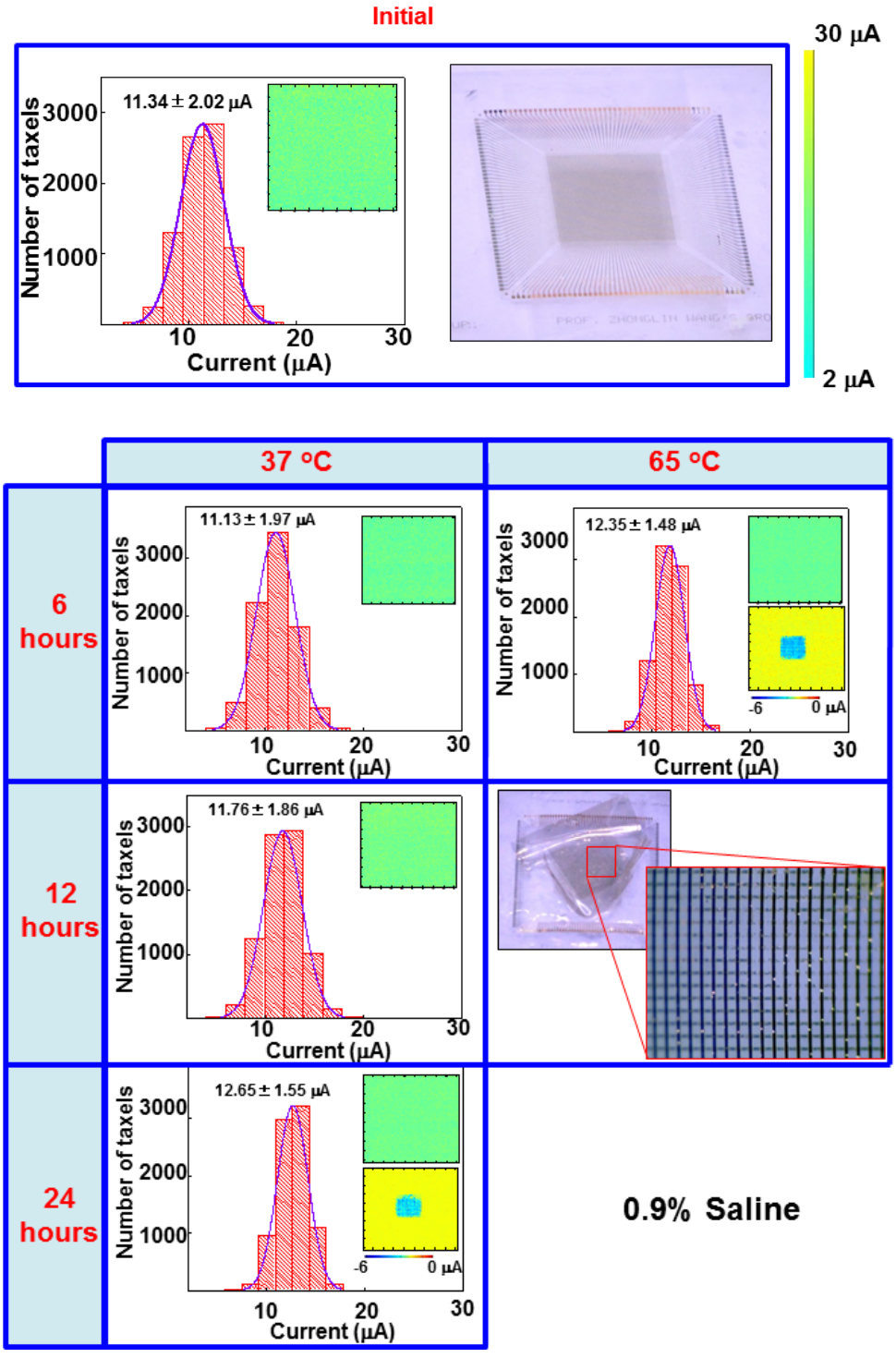

Figure S10: Aging effect of physiological environment on SGVPT array performance. The pressure applied for device after 24 hours in 37 ^{o}C 0.9% saline solution and 6 hours in 65 ^{o}C 0.9% saline solution is ~ 15 kPa.

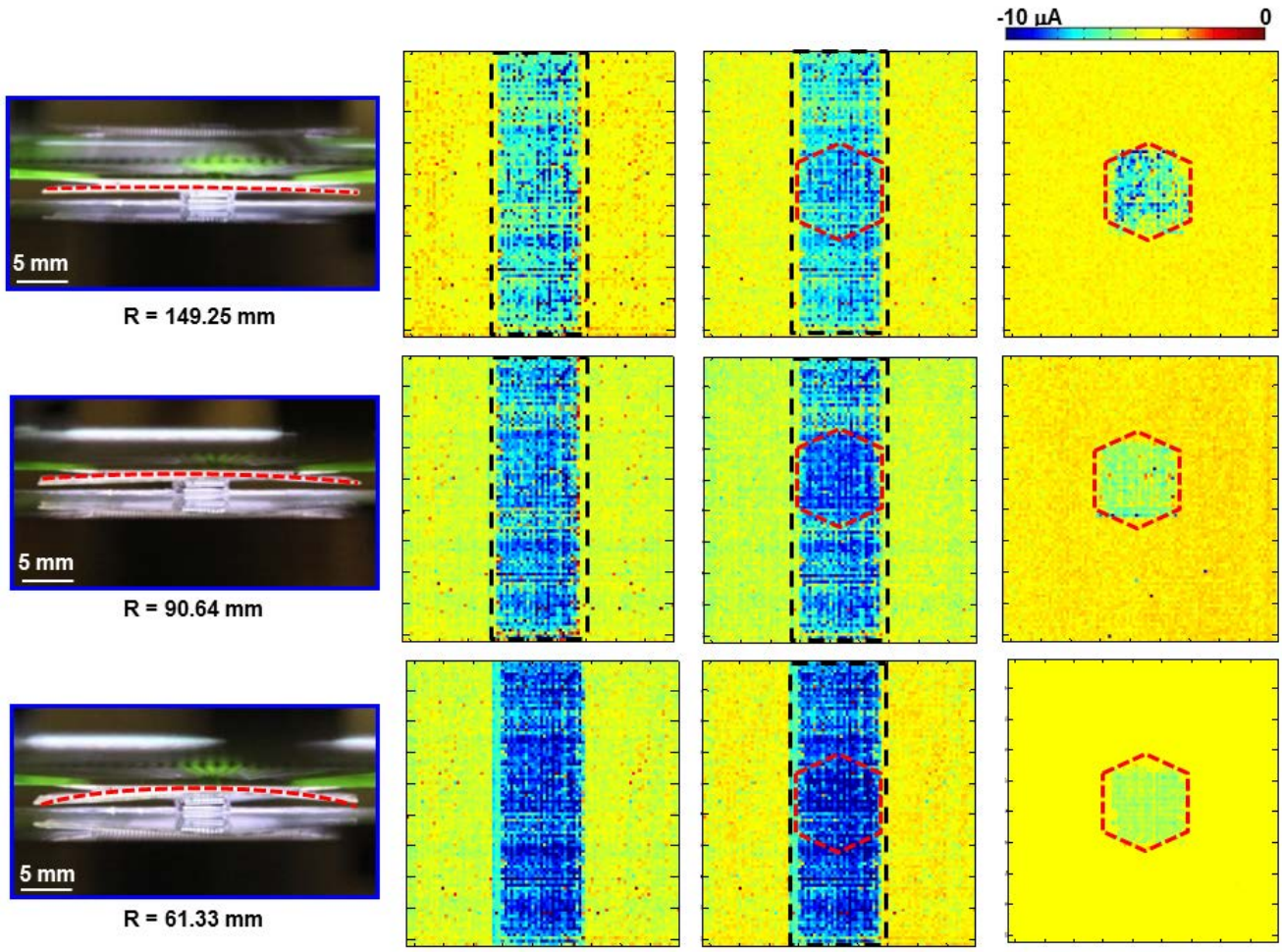

Figure S11: Shape-adaptive sensing for different bending radii.

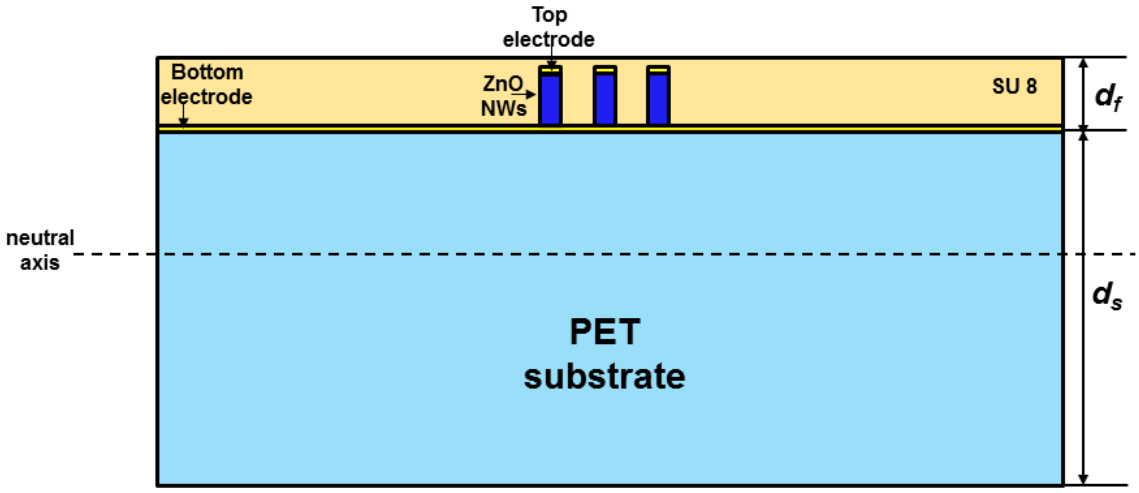

Figure S12: Schematic diagram of analytical model for determining the detectable range of shape-adaptive sensing by SGVPT array.

$$\varepsilon = \left(\frac{d_f + d_s}{2R}\right) \frac{\left(1 + 2\frac{d_f}{d_s} + \frac{Y_f}{Y_s} \times \left(\frac{d_f}{d_s}\right)^2\right)}{\left(1 + \frac{d_f}{d_s}\right)\left(1 + \frac{Y_f}{Y_s} \times \frac{d_f}{d_s}\right)}$$

ε: Generalized plane strain on top surface
d_f, d_s: Thickness of top film (active layer of device) and PET substrate
Y_f, Y_s: Young's modulus of top film and PET substrate

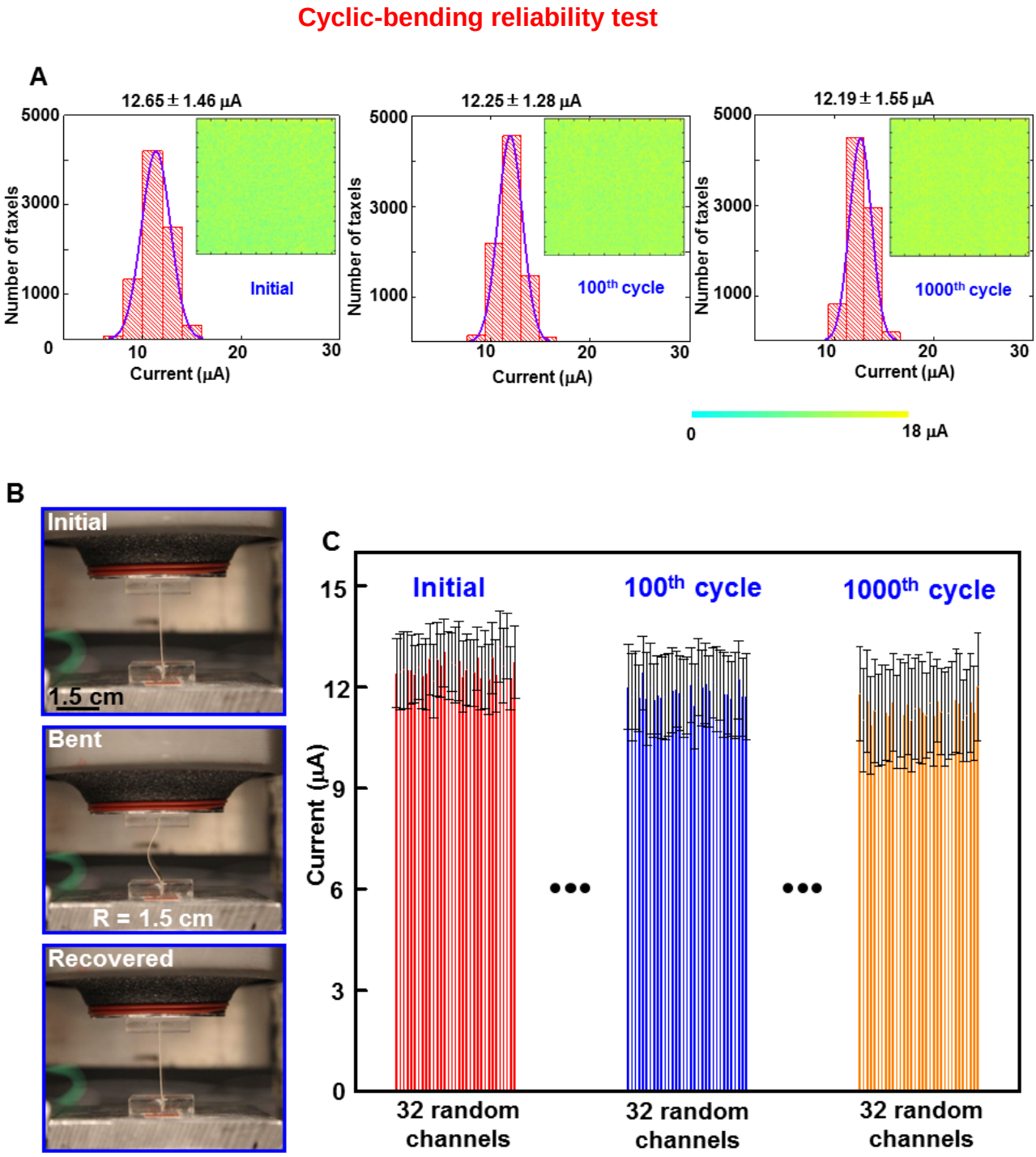

Figure S13: Cyclic test investigating the reliability and stability of SGVPT array operations. Taxel current with 1 V bias for 32 random channels (each with 92 taxels) was monitored and statistically investigated as well as plotted here.

Self-powered active tactile imaging of SGVPT array

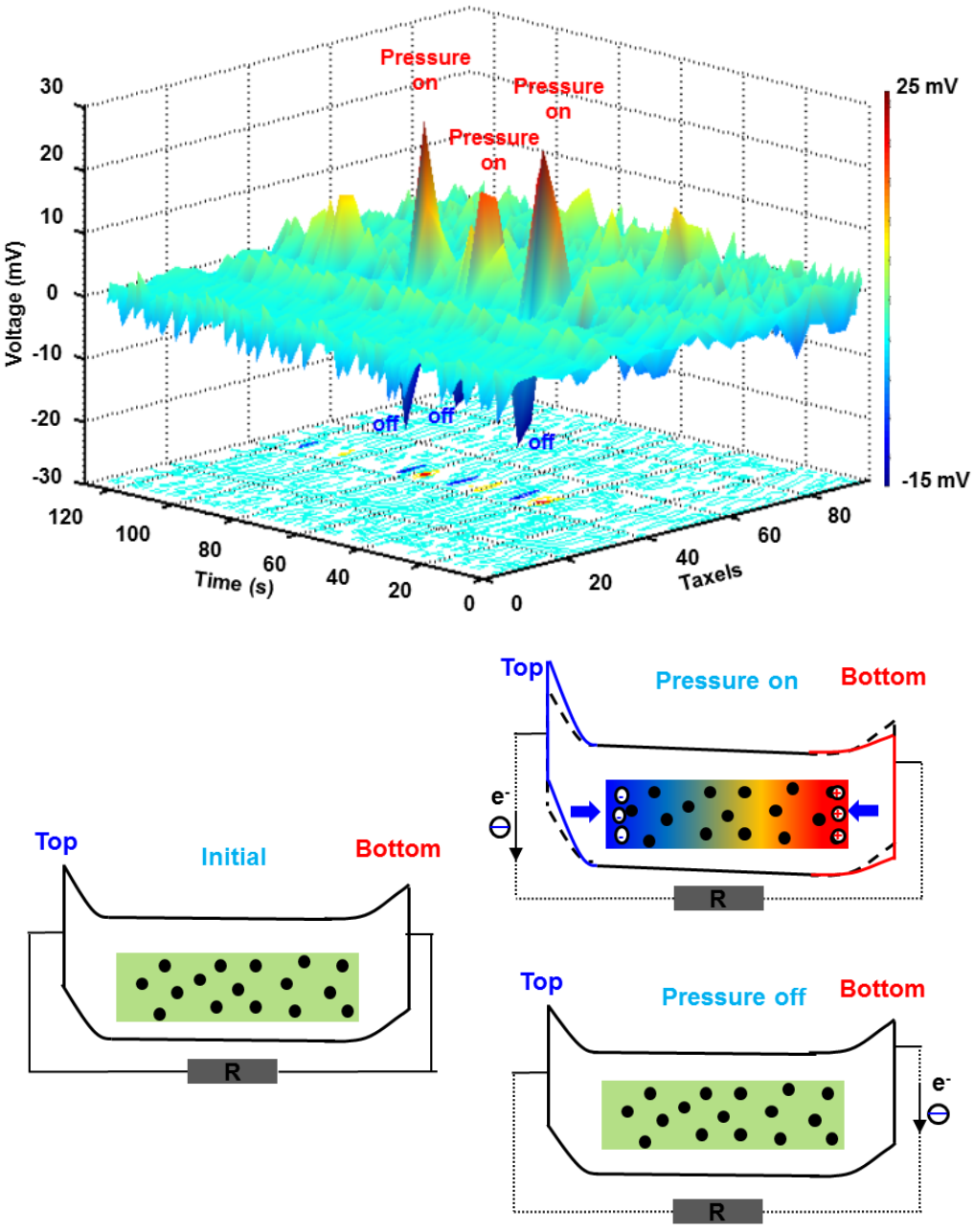

Figure S14: The 3D contour plot at the top presents the measured electrical voltage pulses generated by SGVPT taxels under periodic local pressure, without external applied bias. No observable output voltages can be detected from taxels without applied pressure. The above data obtained from 1 x 92 SGVPT array demonstrates the operation of SGVPT as active sensors for tactile imaging by utilizing piezopotential for

driving flow of electrons in external load, without external bias applied (e.g., the nanogenerator). The band-diagrams at the bottom depict the underlying mechanism of self-powered active tactile sensing by SGVPTs. With normal pressure applied, the negative piezopotential induced at the top Schottky contact of SGVPT can drive the electrons flow from top to bottom contact through external load, which results in the observed voltage pulses (red upward peaks in the above 3D contour plot). When the normal pressure is removed, the accumulated charges can flow back from bottom to top contact through external load, which results in the observed voltage pulses (blue downward peaks in the above 3D contour plot).

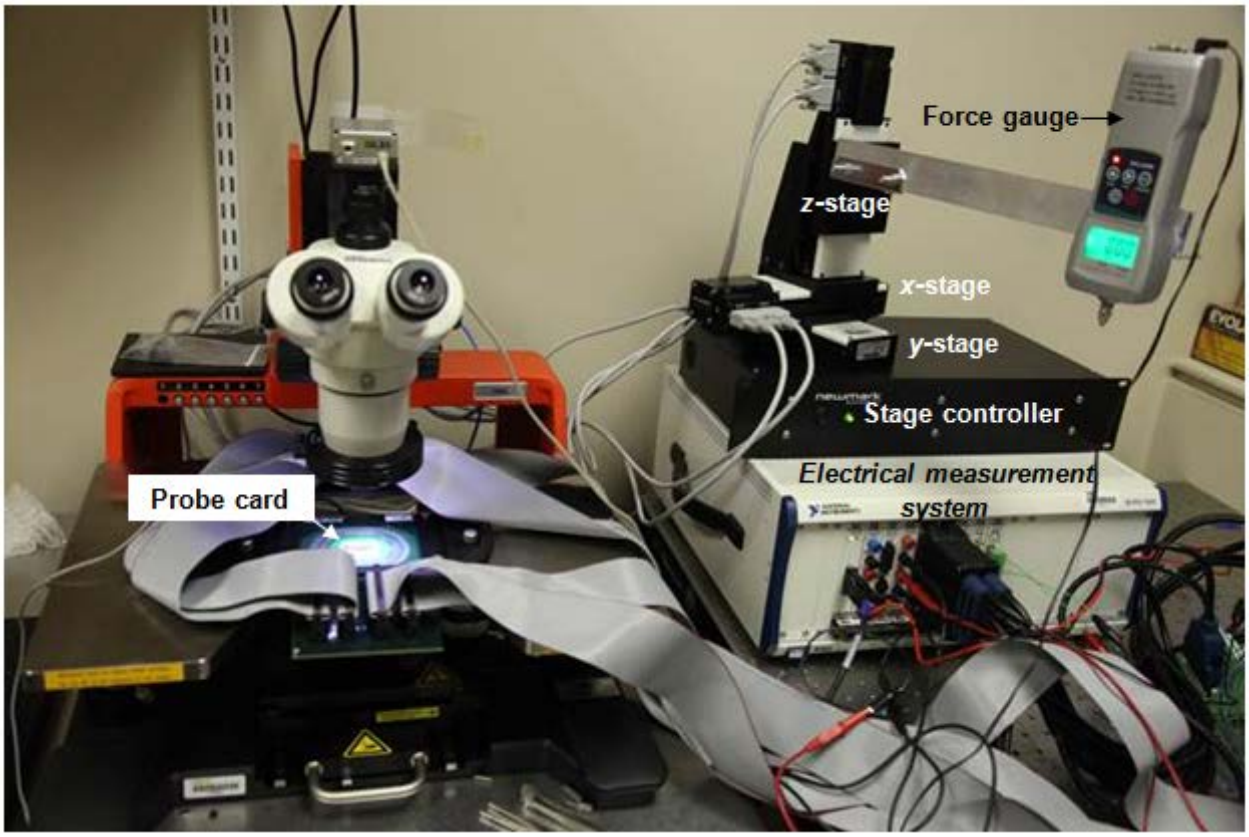

Figure S15: Experimental setup for multichannel multiplexed measurement and programmed mechanical inputs.

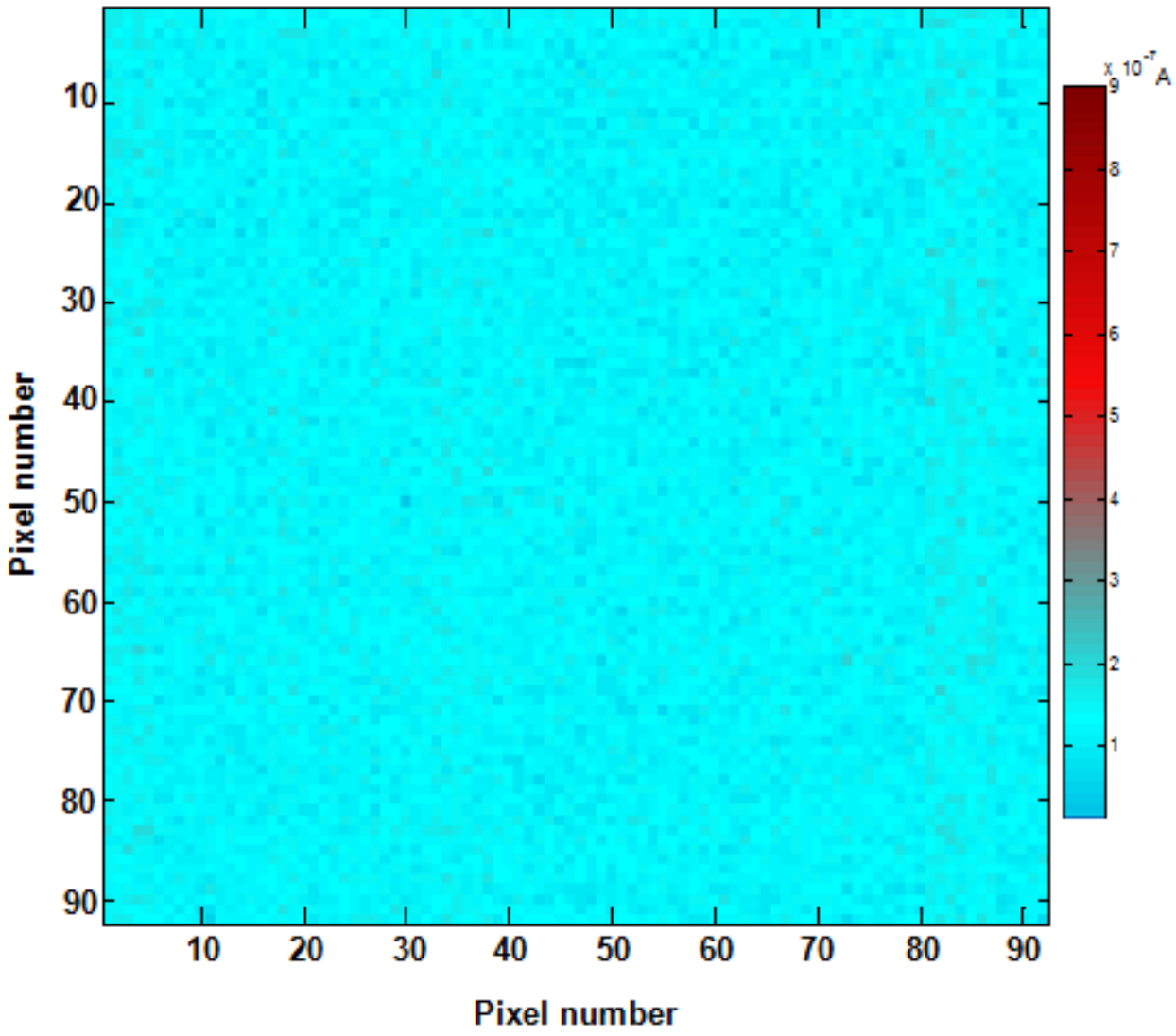

Figure S16. Background noise test for the measurement system under 1 V bias.